Studia Geotechnica et Mechanica
Volume 47 Issue 3 · pp. 46–61 · DOI: 10.2478/sgem-2025-0019

Studia Geotechnica et Mechanica

Bearing capacity of tapered walls: Physical modeling and numerical analysis

Research Article

Worku Firomsa Kabeta*

Faculty of Civil and Environmental Engineering, Department of Geotechnical and Hydraulic Engineering, Gdańsk University of Technology, 11/12 Gabriela Narutowicza St., Gdańsk, 80-233, Poland

Received 05 December 2024; Accepted 22 May 2025

Abstract: This study investigates the load–displacement behavior and failure mechanisms of tapered walls using numerical methods validated against experimental data. A two-dimensional (2D) plane strain approach was adopted to effectively represent the behavior of tapered piles under vertical loading. Finite element method simulations (using both Mohr–Coulomb and hardening Mohr–Coulomb models) and limit analysis with LimitState GEO were employed to analyze three tapered wall configurations with taper angles of 0° (straight wall), 0.75° (moderately tapered), and 1.5° (sharply tapered) in dense sand. The results reveal the significant influence of taper geometry on load-bearing capacity and failure mechanisms, with the moderately tapered wall achieving the optimal balance of shaft friction and base resistance. Numerical predictions underestimated the experimental results by up to 30%, primarily due to installation effects, which were not incorporated into numerical models. This study underscores the necessity of incorporating installation-induced effects for realistic design and modeling of displacement piles.

Keywords: *Tapered piles • Centrifuge • Failure mechanisms • Numerical analysis • Installation effects*

1. Introduction

Tapered piles have gained increasing attention in geotechnical engineering due to their potential for enhancing load-bearing performance in foundation systems. Unlike conventional straight piles, tapered piles have a decreasing cross-sectional area along their length, which can lead to significant improvements in both installation efficiency and load resistance. Understanding the behavior of tapered piles during installation and static loading is essential for optimizing their design and practical applications.

Several studies have demonstrated the effectiveness of tapered piles under different loading conditions. Fahmy and El Naggar [1] and Naggar and Sakr [2] reported significant improvements in bearing capacity for tapered piles due to their ability to concentrate stress more effectively at the base compared to uniform piles. Furthermore, Sakr and Hesham El Naggar [3] and Wei and El Naggar [4] found that tapering enhances shaft friction, a critical factor for achieving optimal performance in sandy soils.

The installation process is also pivotal in determining the performance of tapered displacement piles. They induce soil displacement and compaction, which alter the mechanical properties of the surrounding soil. Randolph et al. [5] demonstrated that soil disturbance during installation significantly affects soil–pile interaction, influencing load–settlement behavior and ultimately dictating pile capacity. In sandy soils, compaction around the pile enhances shaft friction while facilitating the mobilization of base resistance at relatively small displacements [6].

Centrifuge testing has emerged as an effective method to study these interactions, replicating stress and strain conditions in controlled laboratory settings. Centrifuge tests simulate gravitational forces, allowing detailed analyses of pile behavior under diverse loading scenarios without the logistical challenges of field testing. Beijer Lundberg et al. [7] emphasized the value of centrifuge tests in understanding pile installation effects, including load transfer mechanisms and stress distributions.

Numerical analysis is equally essential for predicting the behavior of tapered piles under varying conditions. Installation effects can be possibly considered by various

* *E-mail: worku.kabeta@pg.edu.pl*

numerical methods. These include large-strain finite element method (FEM) [8, 9], coupled Eulerian–Lagrangian methods [10-12], material point method [13-15], and DEM analysis [14, 16, 17]. Simplified approaches like the press and replace method with step-by-step analysis [18, 19] are also used. In this study, a simple FEM approach is used to estimate the bearing capacity of tapered piles under plane strain conditions. Advanced software such as OPTUM G2 enables the simulation of complex soil–structure interactions and material behaviors [20], while LimitState GEO provides analysis of failure mechanisms and collapse patterns [21]. Its capabilities in elastoplastic modeling and limit analysis (LA) provide detailed insights into load–displacement behavior and stress distributions. Notably, OPTUM G2 can estimate both lower (statically admissible solution) and upper (kinematically admissible solution) limit values of bearing capacity, with the upper value being particularly useful for comparison with solutions obtained from LimitState GEO. LimitState GEO software utilizes the discontinuity layout optimization (DLO) method to provide detailed insights into failure mechanisms and collapse patterns [22]. The DLO approach identifies potential slip lines or failure paths in the soil and optimizes their configuration to determine the upper bound solution of the bearing capacity problem. In this study, the Mohr–Coulomb (MC) soil model was employed in LimitState GEO, with input parameters similar to those of FEM.

This work presents that the numerical analysis of displacement piles is incomplete without considering the installation effects of stress and strain distribution in the surrounding soil. The author estimated the upper and lower bound solutions for the bearing capacity of this foundation in the case of non-displacement (wish-in-place or bored) piles and determined the magnitude of the installation factor in the case of plane strain piles in dense sand. If the installation factor for the axisymmetric case was widely studied, the case of plane strain piles (walls) was not considered. The bearing capacity was estimated for the three shapes of model piles embedded in dense sand, simulating with two types of soil model and taking into account different dilatancy angles in the soil mass and at the soil–structure interface. It was found that the choice of an associated flow rule with a high interface angle can substantially increase the calculated soil bearing capacity. The effect of the upper limit (cap) on soil dilatancy within the interface was also examined. In this way, the choice of higher dilatancy within the interface and in the soil mass could increase the bearing capacity of the bored pile and reduce the gap between the numerical modeling and experimental results. The estimated installation factor was higher in the case of the hardening soil model than for the Mohr–Coulomb model.

This study presents part of a broader research effort investigating the installation effects of tapered piles using centrifuge modeling and numerical simulations. The current study focuses specifically on the bearing capacity of tapered piles in sand, based on both experimental data and numerical analysis. While this study quantifies the impact of installation effects on bearing capacity, the associated stress distribution in the surrounding soil has already been presented in our previous work [23]. The effects of installation on strain and displacement fields, examined using particle image velocimetry techniques during centrifuge testing, will be discussed in a forthcoming publication. The findings of this study demonstrate that neglecting installation effects in numerical models leads to a significant underestimation of pile capacity compared to experimental results. This comparison underscores the importance of accounting for installation-induced changes in soil behavior when evaluating the bearing performance of tapered piles.

2. Methodology

This study utilizes a two-dimensional (2D) plane strain approach for modeling tapered walls, which allows for an effective representation of their behavior under various loading conditions. This 2D modeling framework is assumed to represent the behavior of piles, simplifying complex interactions while maintaining accuracy in simulating the load–displacement behavior and failure mechanisms analogous to those observed in axisymmetric pile systems. Three tapered wall types with varying taper angles and having the same volume were analyzed using FEM and LA. The geometry of the model walls in the centrifuge container was replicated in the numerical models.

2.1 Centrifuge modeling

A series of centrifuge tests were conducted at the Geotechnical Centrifuge Facility of Gustave Eiffel University to replicate field stress conditions and study the behavior of tapered piles. These tests aimed to provide insights into the performance of tapered piles and walls in dense sand during installation and static loading.

2.1.1 Test setup

The experiments were conducted using a strongbox container measuring 800 mm × 450 mm × 200 mm, filled with dense Fontainebleau NE34 sand. The sand was prepared using the sand raining technique to achieve a uniform relative density of 68%. Figure 1 illustrates the preparation process, including the sand raining technique and the prepared container.

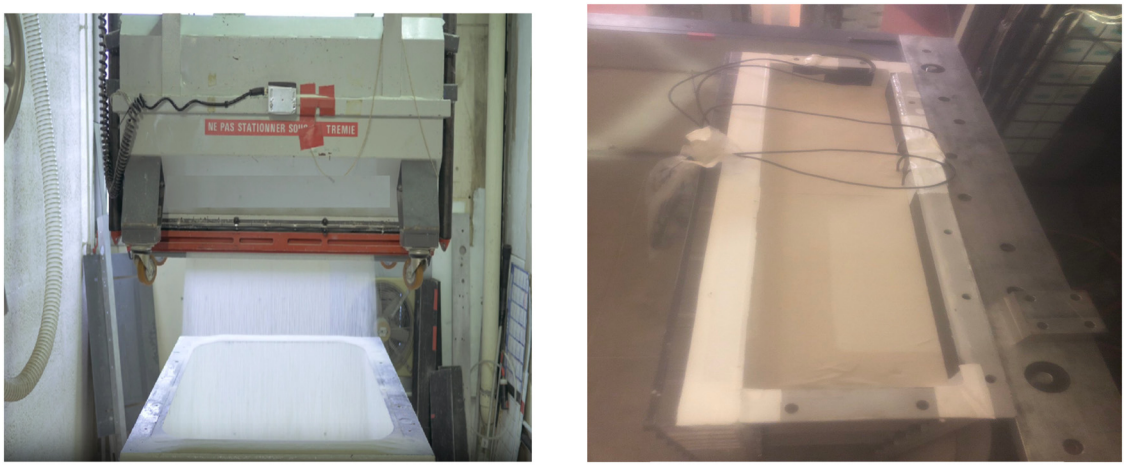

Figure 1. Sand preparation process: (a) sand raining technique and (b) prepared strongbox.
Source: Author's contribution.

Three model walls with varying taper angles were fabricated for testing: a straight wall (S) with a 0° taper and a bottom width of 16 mm, a moderately tapered wall (T1) with a 0.75° taper and a bottom width of 12 mm, and a sharply tapered wall (T2) with a 1.5° taper and a bottom width of 9 mm. The top widths were 16 mm for *S*, 19 mm for T1, and 22 mm for T2. All walls were 224 mm in embedded length and made from steel. The layout of the experimental setup and positioning within the container is depicted in Figure 2, which provides a section view (Figure 2a) and a plan view (Figure 2b).

2.1.2 Experimental procedure

The sand was placed in a strongbox container, and the model walls were carefully positioned in the loading

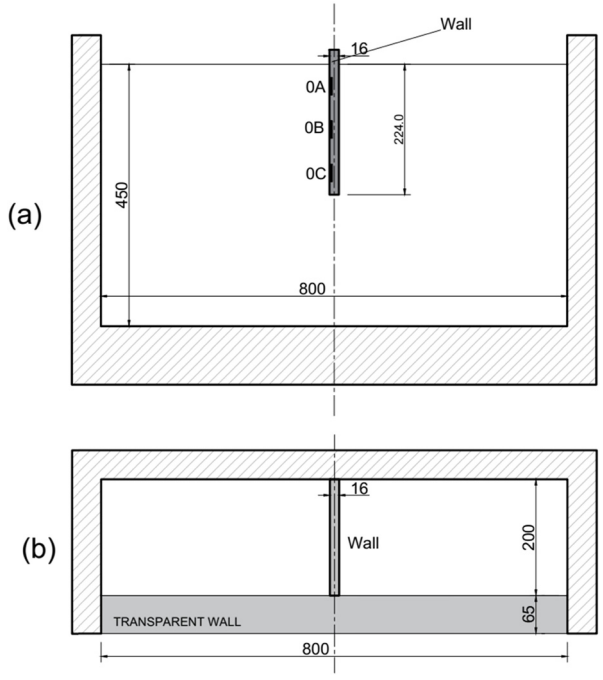

Figure 2. Experimental setup layout: (a) section view and (b) plan view at the end of wall installation. All dimensions in mm.
Source: Author's contribution.

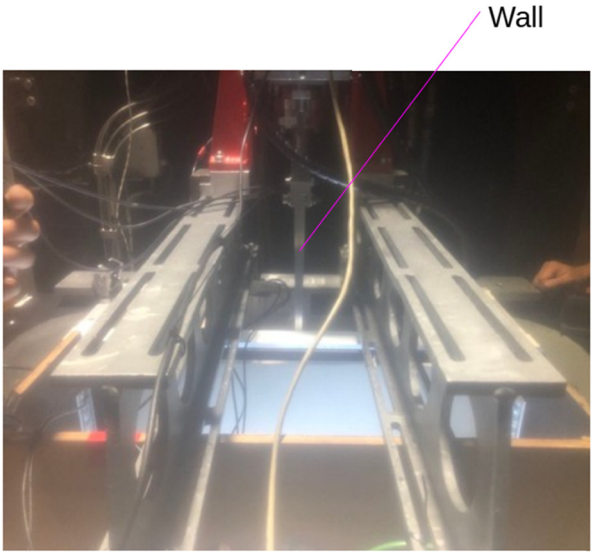

Figure 3. Experimental setup with model walls and loading frame configuration.

Source: Author's contribution.

frame with their bases near the soil surface (Figure 3). The centrifuge was operated at an acceleration of 25 *g* to replicate field stress conditions. During the installation phase, the walls were pushed into the sand at a constant penetration rate of 0.1 mm/s until a depth of 224 mm was reached. Displacement and load data were continuously monitored throughout the process to ensure accuracy. Following the installation, static loading tests were performed in compression and tension. The vertical load was applied at a constant rate of 0.1 mm/min until the pile settlement reached its base diameter (16 mm for the straight wall).

2.2 Numerical analysis

Numerical simulations were conducted to complement the experimental findings and provide further insights into the load–displacement behavior and failure mechanisms of tapered walls. Two numerical approaches were employed: the FEM using OPTUM G2 and the LA using LimitState GEO.

2.2.1 FEM

2.2.1.1 Model setup

A 2D plane strain model was developed for the three types of walls used in the experiment. The model dimensions were defined as 800 mm width (*B*) and 450 mm height (*H*) to replicate the container size used in the centrifuge tests (Figure 4).

The straight wall (*S*) has a constant breadth (*b*) of 16 mm, while the tapered walls (T1 and T2) were designed to have equivalent volumes. For T1, the bottom breadth was 13 mm, increasing to 19 mm at the top, and for T2, the bottom breadth was 10 mm, increasing to 22 mm at the top. They were characterized by a smaller base area compared with a straight wall. As the end-bearing mechanism dominates in the bearing capacity, the lower base area of tapered walls will not compensate for the increased lateral friction mobilized on the wall [23]. All walls are embedded in the soil to a depth (*h*) of 224 mm.

2.2.1.2 Material properties

The soil behavior was represented using both MC and hardening Mohr–Coulomb (HMC) models, which account for different stress–strain responses under loading. The HMC model offers a significant advantage over the traditional MC model by incorporating strain-hardening and strain-softening behavior, allowing for a more accurate representation of the progressive development of plastic strains under loading [24]. This feature is particularly useful for modeling dense sands, where the stress–strain response is characterized by initial hardening followed by softening due to dilatancy and eventual shear failure. In contrast, the MC model assumes perfect plastic behavior beyond the yield point, which can oversimplify the actual soil response. The piles were modeled as rigid materials.

The parameters for Fontainebleau sand were taken based on experimental tests by Andria-Ntoanina et al. [25], as shown in Table 1. For the non-associated flow rule in the HMC model, the Taylor flow rule was applied with a dilatancy angle of 5.37°, while in the MC model, a

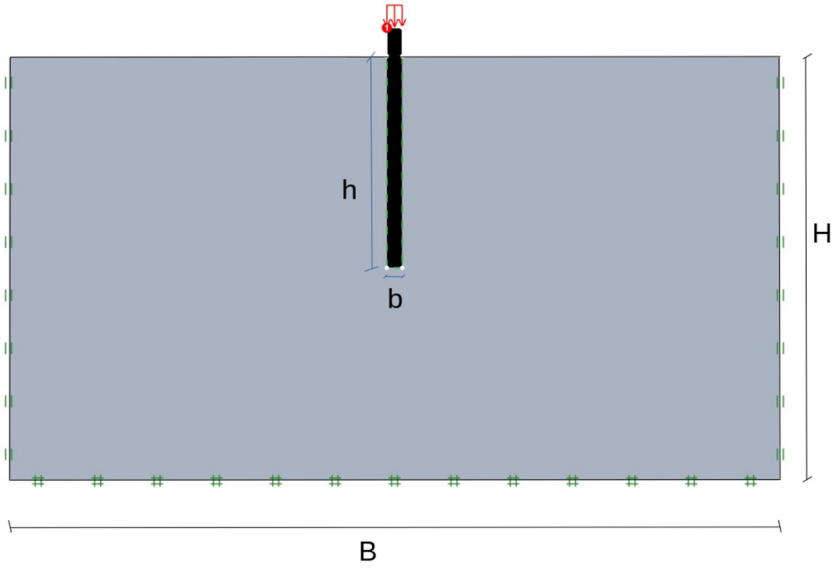

Figure 4. Numerical model setup in OPTUM G2.

Source: Author's contribution.

dilatancy angle of 5° was assumed. The effect of considering volumetric dilation cap was analyzed by assuming a unit value for the dilatancy in the non-associated flow rule of the MC model. The interface material has the same properties as the soil but with a reduced friction angle of 16° to account for lower resistance at the interface. The centrifuge experiment on a model scale was considered in numerical analysis. The unit weight of the soil used in simulations was thus multiplied by a factor of 25 to account for increased gravity during centrifuge tests, resulting in an effective unit weight of 400 kN/m^3. Additionally, the rigid wall was assumed with a unit weight of 1,750 kN/m^3.

2.2.1.3 Analysis type

OPTUM G2 was used to perform FEM simulations. The initial analysis focused on a standard wall (S), examining the effects of various parameters such as boundary size, mesh density, associated and non-associated flow rules, and the inclusion of a dilation cap on the load–displacement behavior. Both the MC and HMC models were employed, with the MC model analyzed under both associated and non-associated flow rules to account for their differing effects on load capacity.

The effect of a dilation cap was also analyzed for the non-associated MC model, as it influences the volumetric

Property	MC model	HMC model
Young's modulus (E)	35 MPa	
Friction angle (φ')	31.5°	31.5°
Cohesion (c')	0	0
Poisson's ratio (ν)	0.3	0.3
Unit weight (γ)	16 kN/m^3	
Reference Young's modulus ($E_{50,ref}$)		40 MPa
Unloading modulus ($E_{ur,ref}$)		75 MPa
Earth pressure coefficient (K_0)	0.47	0.47
Dilatancy angle for non-associated flow (ψ)	5.0°	5.37°
Reference stress (p_{ref})		100 kPa
Hardening parameter (m)		0.5

Table 1. Properties of sand used in OPTUM G2 analysis [25].

Source: Author's contribution.

response of the soil during loading. Static loading was applied incrementally until the pile settlement reached its base diameter (16 mm for the straight pile). The output from the FEM simulations is the load–displacement curve, which was analyzed under different scenarios, including variations in the taper angle, changes in mesh density, and behavior model for soil and interface.

2.2.2 LA

LA was conducted using LimitState GEO to investigate the failure mechanisms and failure loads of the tapered piles.

2.2.2.1 Model setup

For consistency with the FEM simulations and the experimental setup, a 2D model similar to that used in FEM (Figure 4) was created for each wall. The model dimensions, geometry, boundary conditions, and material properties were identical to those in the FEM analysis. The soil behavior in the simulations was represented using the MC model with the associated flow rule. These properties were adopted from FEM analysis to ensure consistency across the numerical methods.

2.2.2.2 Analysis type

The LA simulations were aimed at identifying the kinematic failure mechanism and collapse loads for each wall type. The analysis assumed static loading and modeled the pile failure process by analyzing how the soil behaves under increasing loads. Mesh resolution sensitivity tests were performed to assess the accuracy of the failure mechanisms. From LA, the effect of taper angle on the failure mechanisms was assessed. Additionally, failure load comparisons were made between each wall, and the results were compared with the experimental data.

3. Results

3.1 Centrifuge test results

The results of centrifuge tests, including stress distribution in the soil mass, along the pile wall, and installation force–displacement behavior, were presented in Bałachowski et al. [23]. The models were continuously pushed into the sand mass, and this process was performed in-flight. The total force mobilization during wall installation was examined for each wall configuration (Figure 5). It was observed that the total force required for the monotonic installation was slightly lower for the walls with higher taper angles compared to the straight one (S). At a final embedment depth, the penetration force for the sharply tapered wall (T2) was approximately 75% of the axial force required for the straight wall (S), while the moderately tapered wall (T1) required about 90% of the axial force of the straight wall.

3.2 Numerical results

3.2.1 FEM analysis

OPTUM G2 was used to perform FEM simulations. The initial parametric analysis (Figures 6–10) was conducted on a standard straight wall, examining several factors such as the impact of boundary size on load–displacement curves, the effect of associated and non-associated flow rules on the wall performance, the role of the dilation

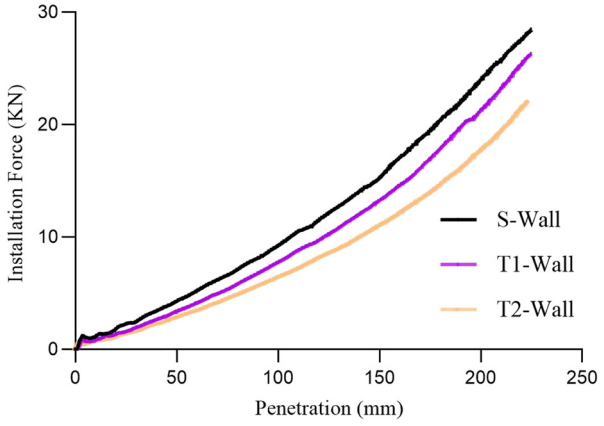

Figure 5. Load at pile head–displacement curves of walls from centrifuge experiments during the installation phase.
Source: Author's contribution.

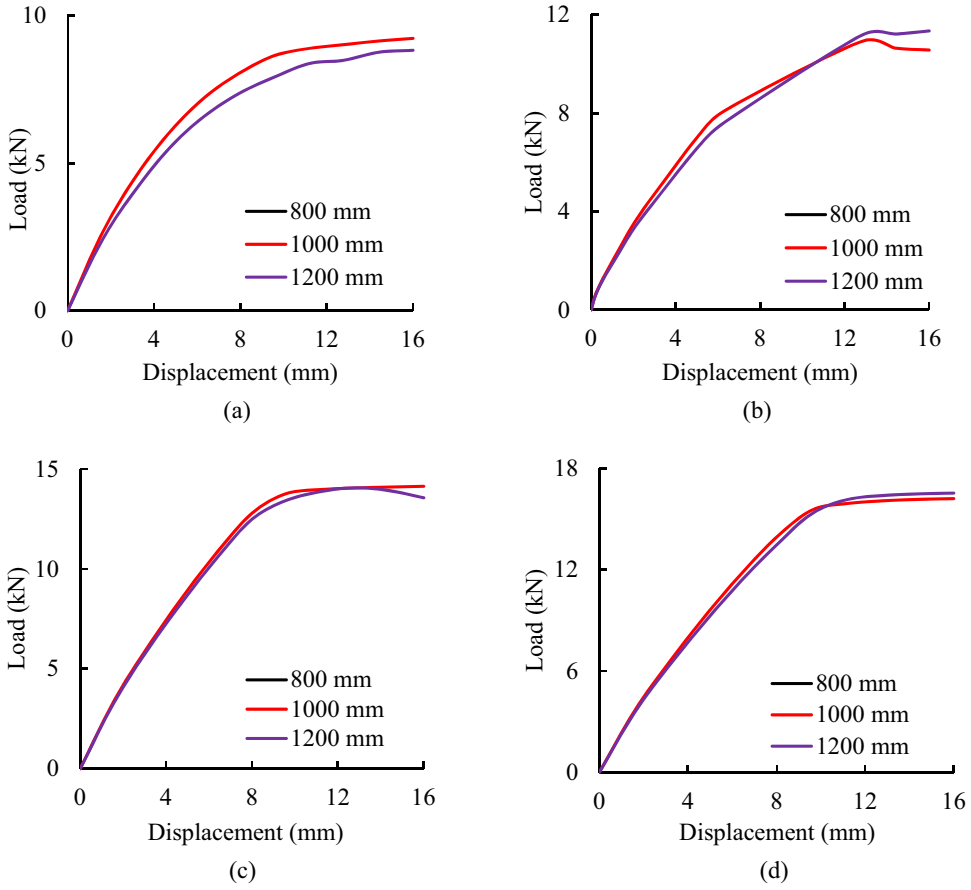

Figure 6. Effect of boundary conditions (container size) on the load–displacement curves: (a) HMC – lower bound, (b) HMC – upper bound, (c) MC – lower bound, and (d) MC – upper bound.

Source: Author's contribution.

cap, and the influence of mesh density. Additionally, the comparison between the MC and HMC models was also considered. Following this, the analysis was extended to tapered walls, focusing on how the taper angle affects the load–settlement behavior. For the load–displacement curves, the head load was calculated by multiplying the stress at the top of the wall by the area of the wall (breadth × length). The wall length for all types was 20 cm (Figure 2b). The following sections present the results of FEM analysis, which address these key topics. The walls were modeled as wish-in-place at a depth of 224 mm (model scale), so the installation effects related to model continuous penetration in the sand mass were not taken into consideration.

3.2.1.1 Effect of boundary size

The influence of the container size on the load–displacement behavior was investigated using FEM analysis. While maintaining a constant domain height of 450 mm, the domain lengths were varied at 800, 1,000, and 1,200 mm. For this case, the mesh density of 1,000 elements was considered. The results, presented in Figure 6, show the load–displacement curves for both the upper and lower bound values obtained from the HMC and MC models with associated flow rules. These results indicate that the variation in the domain size has a negligible impact on the load–displacement behavior, suggesting that boundary effects are minimal under these conditions. Moreover, the lower and upper bound solutions are relatively close to each other.

3.2.1.2 Effect of the number of mesh elements

The influence of mesh density on FEM results was analyzed considering four mesh densities: 1,000, 2,000, 4,000, and 6,000 elements. The effects were examined for both the upper and lower bounds of the HMC and MC models (Figure 7). The analysis shows that as the number of

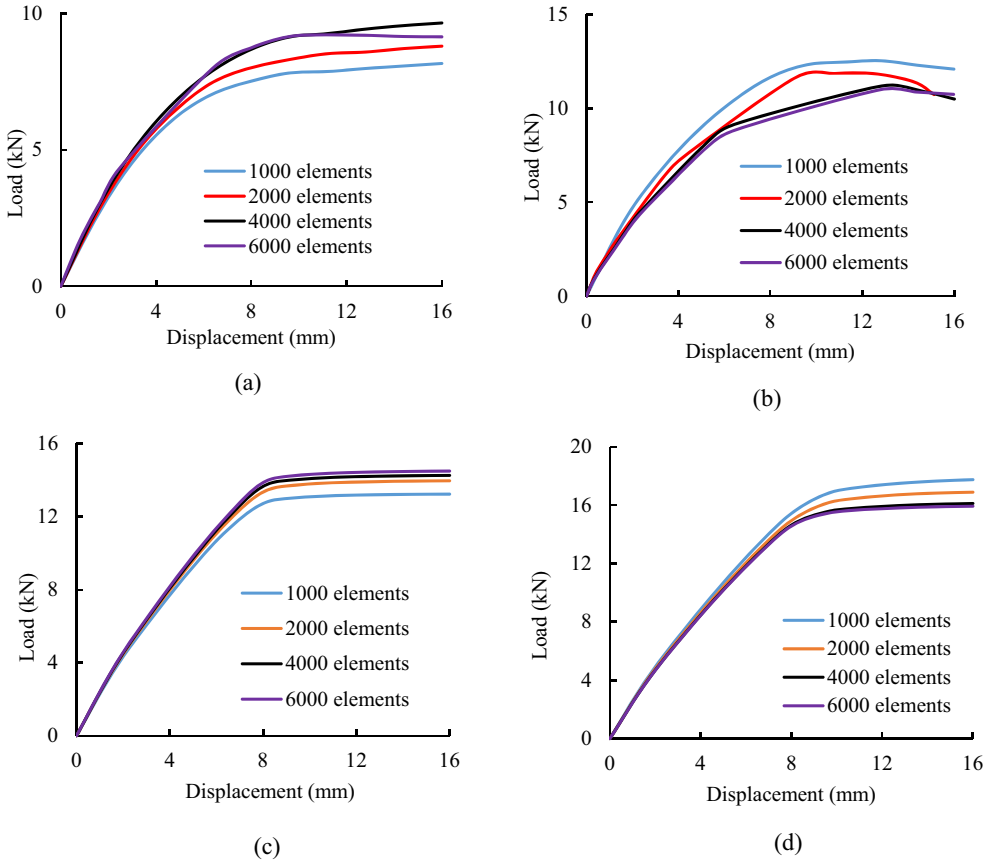

Figure 7. Effect of mesh density on load–displacement curves: (a) HMC – lower bound, (b) HMC – upper bound, (c) MC – lower bound, and (d) MC – upper bound.

Source: Author's contribution.

elements increased, the gap between the upper and lower bounds consistently decreased up to 4,000 elements. Specifically, the lower bound values increased, while the upper bound values decreased, indicating a convergence of results. Beyond 4,000 elements, for example, at 6,000 elements, this effect became negligible, suggesting that further mesh refinement did not significantly improve the solution (Figure 7) but may propagate some numerical

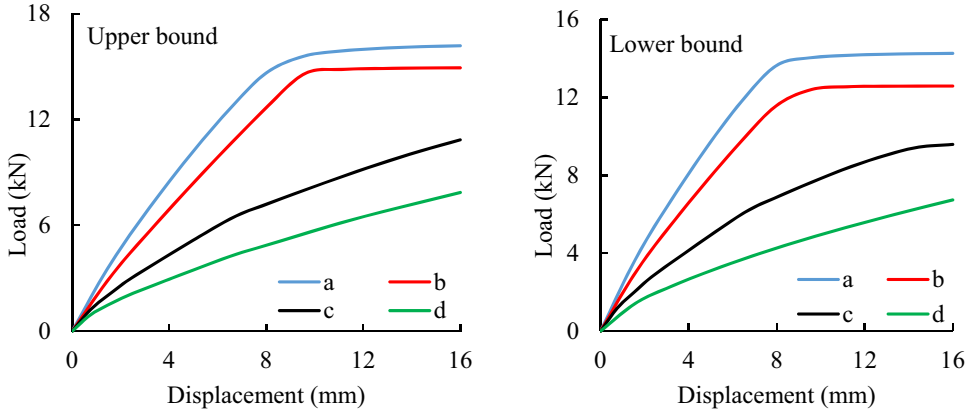

Figure 8. Load–displacement curves for different combinations of MC models with associated and non-associated flow rules.

Source: Author's contribution.

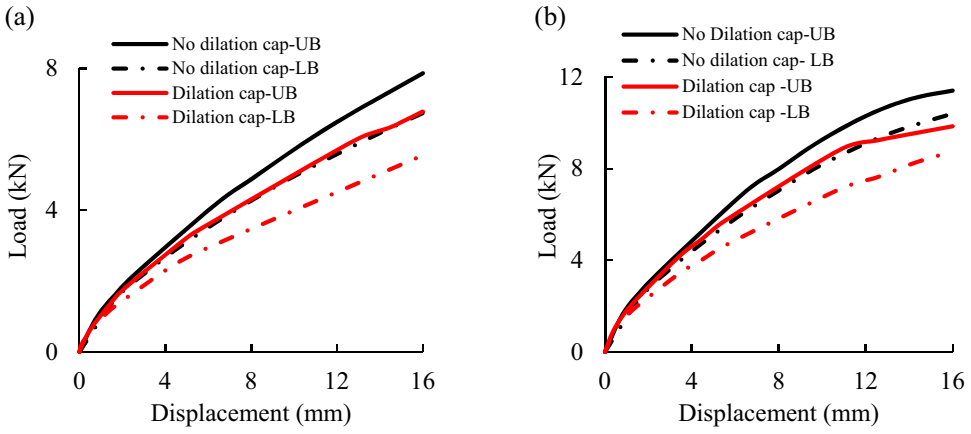

Figure 9. Effect of dilation cap on the load–settlement curves using (a) HMC model and (b) MC model.
Source: Author's contribution.

errors. Thus, the domain of 800 mm with 4,000 elements was assumed for further analysis.

3.2.1.3 Effect of associated and non-associated flow rules for the MC model

The difference between associated and non-associated flow rules within the MC model for the sand mass and wall–soil interface was also investigated. Four cases were considered: (a) associated flow rule for both soil and interface, (b) associated flow rule for soil and non-associated flow rule for the interface, (c) non-associated flow rule for soil and associated one for the interface, and (d) non-associated flow rule for both soil and interface. The results revealed that cases with associated flow rules (a and b) exhibited higher stiffness and load capacity. Among these, case a (associated soil and interface) showed the highest response, followed by case b (associated soil and non-associated interface). Conversely, cases with non-associated flow rules (c and d) exhibited load–displacement behavior with lower stiffness and capacity compared to cases with associated flow rules. Case c (non-associated soil and associated interface) demonstrated higher capacity than case d (non-associated soil and interface), with case d yielding the lowest load capacity among all. These trends are illustrated in Figure 8, where all load–displacement curves (a–d) present a significant influence of flow rules on the predicted wall performance.

3.2.1.4 Effect of dilation cap

The effect of considering a dilation cap was investigated for both the non-associated MC model and the HMC model. In this analysis, a volumetric dilation ($\varepsilon_{v,cr}$) of unit value was applied to both the soil and soil–wall interface. The results indicated that the inclusion of the dilation cap led to slightly lower load–settlement curves compared to cases without the dilation cap in both the MC and HMC models (Figure 9). The dilation cap was not applied in further analysis.

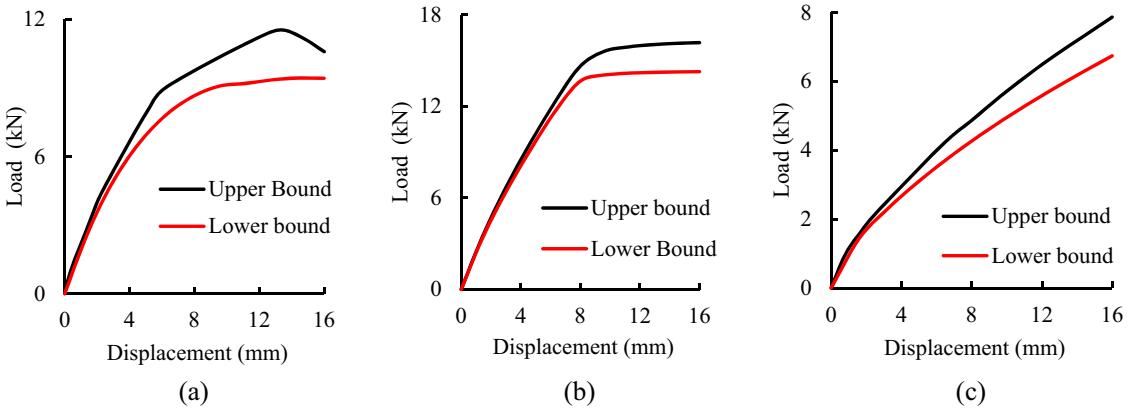

Figure 10. Load–displacement curves of the S wall using (a) HMC model, (b) associated MC model, and (c) non-associated MC model.
Source: Author's contribution.

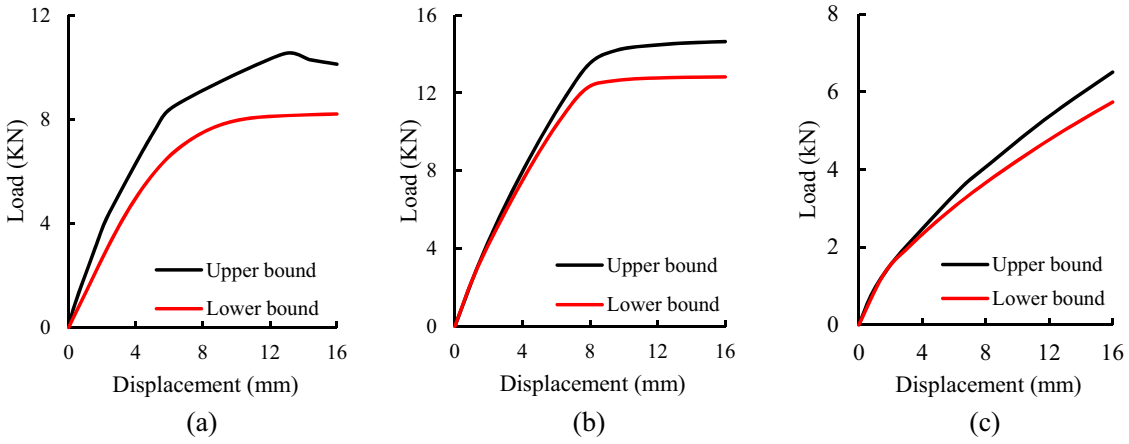

Figure 11. Load–displacement curves for the T1 wall using (a) HMC model, (b) associated MC model, and (c) non-associated MC model. Source: Author's contribution.

3.2.1.5 MC and HMC models

FEM analysis using OPTUM G2 shows distinct differences in load–displacement behavior between the MC and HMC models. The MC model with an associated flow rule provided a baseline representation, capturing linear-elastic behavior followed by plastic deformation at failure. In contrast, the HMC model, with its ability to simulate strain hardening and softening, offered more accurate predictions of soil behavior at higher settlements. This distinction is evident in the load–displacement curves (Figure 10), where the HMC model produces a smoother transition to failure compared to the MC model. The MC solution with a non-associated flow rule gives much softer load mobilization without a distinct failure load as the soil dilatancy is limited.

3.2.1.6 Modeling of tapered walls

After parametric studies concerning the standard wall, the focus was extended to the analysis of tapered walls (T1 and T2). A mesh density of 4,000 elements was adopted, based on the findings from the standard walls, as it provided optimal accuracy and convergence. A container size of 800 mm, consistent with the experimental setup, was used, given the negligible impact of boundary conditions previously established.

The results are presented as load–displacement curves for each tapered wall (Figures 11 and 12). For both walls, three sets of results are shown: HMC, associated MC, and non-associated MC models. The associated MC model consistently produced the highest load capacities due to its assumption of full dilation, followed by the HMC model.

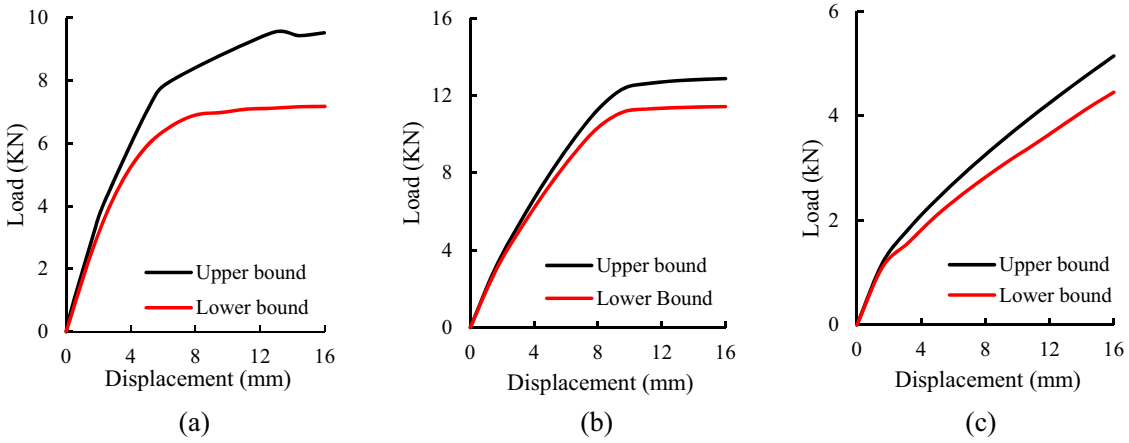

Figure 12. Load–displacement curves for the T2 wall using (a) HMC model, (b) associated MC model, and (c) non-associated MC model. Source: Author's contribution.

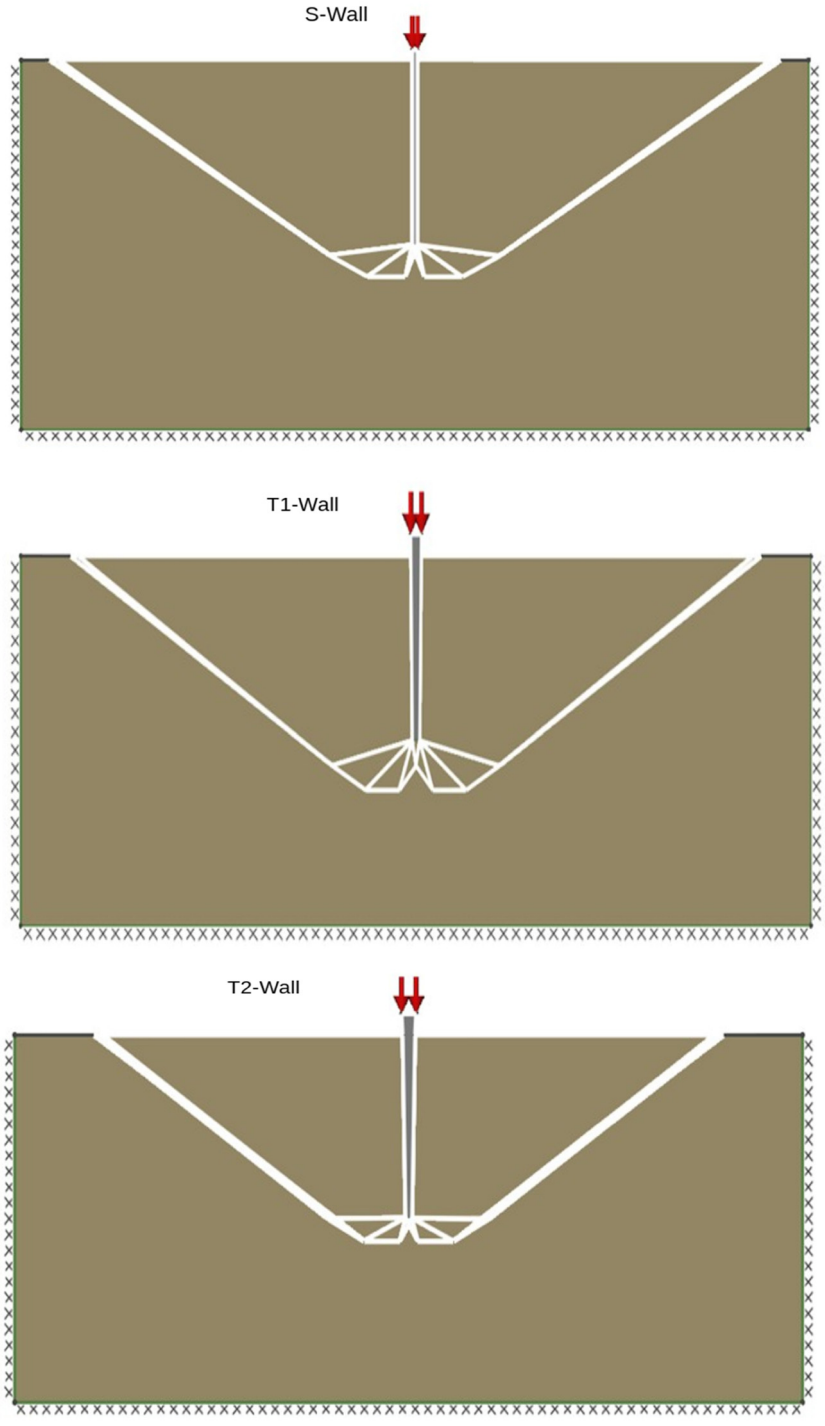

Figure 13. Failure mechanisms of the straight (S), moderately tapered (T1), and sharply tapered (T2) walls.
Source: Author's contribution.

The non-associated MC model yielded the lowest load capacities due to the reduced dilation angle. The HMC model, by incorporating stress-dependent variations in soil stiffness, provided a balanced and realistic prediction of load capacity. The T1 wall exhibited relatively higher load capacity compared to the T2 wall, reflecting the benefits of a moderate taper angle in balancing shaft friction and base resistance.

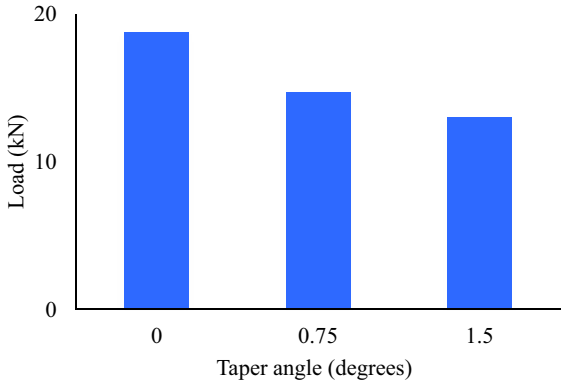

Figure 14. Failure load comparison for S, T1, and T2 walls at the end of installation.

Source: Author's contribution.

3.2.2 LA

LA was employed to investigate the effect of taper angles on the failure load and failure mechanisms of each wall under static loading. This analysis provided insights into the impact of wall geometry on load-bearing capacity and the development of slip surfaces. The soil was modeled using the MC failure criterion with the associated flow rule. The parameters used for the soil were the same as those used in the FEM analysis.

3.2.2.1 Failure mechanisms

The failure mechanisms of the straight wall (S), moderately tapered wall (T1), and sharply tapered (T2) were analyzed to evaluate the effect of taper geometry on failure patterns. For all models, the failure mechanisms exhibited a deep failure mode, with slip lines concentrated near the wall base, extending into the surrounding soil (Figure 13). The results consider upper-bound solution with a kinematic mechanism.

For the straight model (S), the slip lines were localized directly below the base and extended vertically downward, reflecting a concentrated stress zone typical of uniform geometry. This failure mechanism resulted in limited mobilization of the surrounding soil, with the load primarily transmitted by end-bearing at the wall base. The moderately tapered model (T1) displayed a more distributed failure pattern. The slip lines emanated from the base but extended outward along the taper region, indicating enhanced soil mobilization and redistribution of stresses due to the taper angle. This mechanism increased the contribution of shaft friction to the overall load-bearing capacity while maintaining stability near the base. The sharply tapered model (T2) showed a similar deep failure mode but with slip lines concentrated closer to the pile tip and a reduced outward spread. The pronounced taper angle led to higher stress concentrations at the base and shaft. However, due to a smaller base area, this resulted in lower bearing capacity compared to the T1 wall.

3.2.2.2 Failure loads

The failure loads at the end of installation for the three wall types were evaluated (Figure 5) and are compared in Figure 14. The straight wall (S) achieved the highest failure load of 18.78 kN, followed by the moderately tapered (T1),

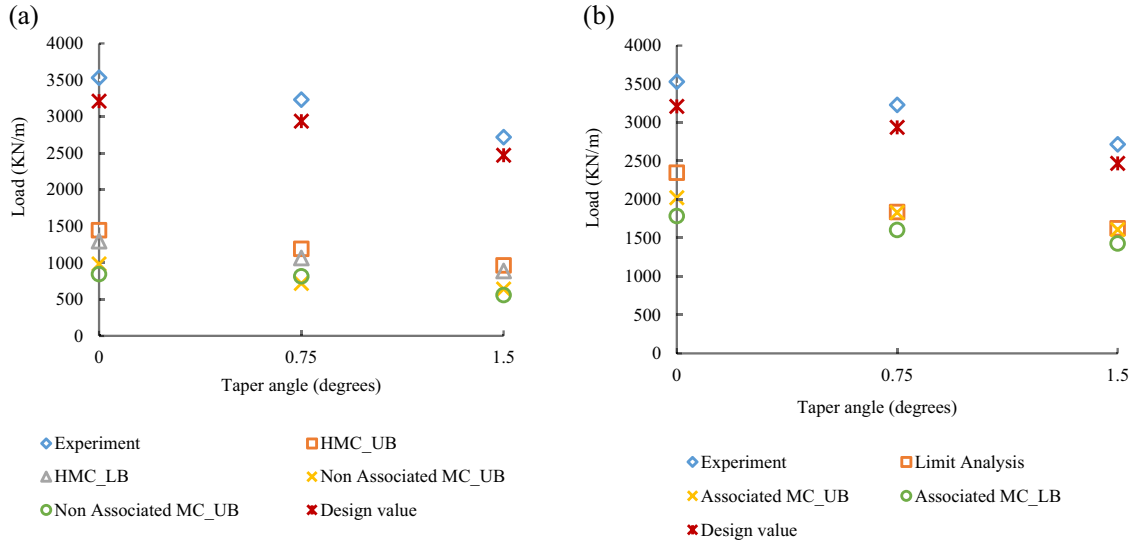

Figure 15. Comparison of numerical and experimental analysis (prototype scale) for (a) non-associated flow rule and (b) associated flow rule.

Source: Author's contribution.

which reached 14.68 kN. The sharply tapered wall (T2) exhibited the lowest failure load of 12.9 kN. This trend is consistent with the findings from FEM analysis, confirming the substantial effect of pile geometry on load capacity. The results emphasize that while the straight pile (S) offers the greatest load-bearing capacity due to its largest base area, moderate tapering in the T1 pile provides a balance between the base capacity and soil–wall interaction. In contrast, excessive tapering in the T2 pile significantly reduces load capacity due to stress concentrations and reduced base area.

3.3 Comparison of numerical results with the experimental data

To validate the FEM and LA models, numerical results were compared with centrifuge test data at the end of monotonic penetration. It is essential to note that the walls in the numerical models were analyzed as wish-in-place, meaning the installation effects were not considered. During the centrifuge experiments, the walls were progressively pushed into dense sand, inducing significant stress and deformation changes in the surrounding soil. These changes, including densification, displacement, and stress redistribution, substantially enhanced the load-bearing capacity observed in the experiments. Figure 15 shows a summary of the upper bound solution obtained from the FEM analysis (both MC and HMC models), LA, and centrifuge experimental results. For clarity of presentation, the results are given in prototype scale for 1 m of continuous wall. The design value of head load from centrifuge tests was estimated according to EC-7 standard based on physical modeling results and Design Approach 2 (DA2). The characteristic value of head load at the end of continuous penetration was divided by the bearing capacity partial factor for compression piles (γ_t = 1.1). The correction coefficients for the bearing capacity of piles subjected to axial loading based on static load tests ($\xi 1$, $\xi 2$) were assumed to be 1.0.

The LA results consistently predicted higher load values than FEM models. However, even the highest LA predictions were below the experimental values, which shows the critical influence of installation effects. The MC-associated flow rule provided the upper bound for load predictions, showing higher values compared to the MC non-associated and HMC models. FEM provides detailed predictions of load–displacement behavior and deformation mechanisms, while LA focuses on failure mechanisms and collapse loads.

To further investigate the impact of installation, relative installation effects were calculated by comparing the experimental ultimate loads with numerical results, as shown in equation (1):

$$\text{Relative installation effect (\%)} = \frac{\text{Experimental value} - \text{Numerical solution}}{\text{Experimental value}} \times 100, \quad (1)$$

$$\text{Numerical solution} = \frac{\text{Upper bound value} + \text{Lower bound value}}{2}. \quad (2)$$

Figure 16 illustrates the relative installation effects of walls with their respective taper angles. The results indicate that the relative installation effects vary significantly depending on the analysis method and taper angle. The MC-non-associated model consistently gives the highest relative installation effect, close to 75%, followed by the HMC model with relative effects close to 65%.

In contrast, the MC-associated model and LA gave lower relative installation effects. Specifically, the LA

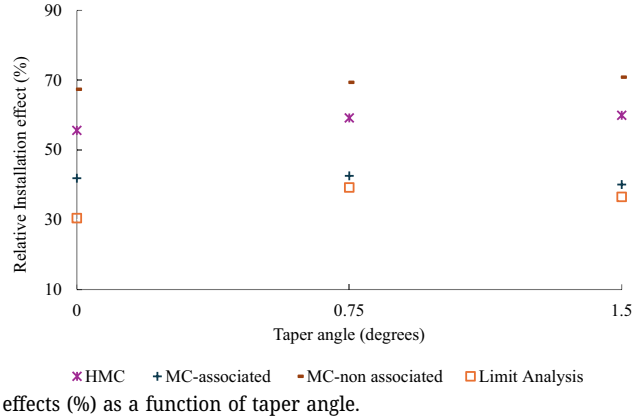

Figure 16. Relative installation effects (%) as a function of taper angle.

Source: Author's contribution.

solution presents the values closest to the experiment with the lowest relative installation effect of about 35–40%. The relative installation effect tends to increase with taper angle. These variations emphasize that taper geometry and the choice of analysis method significantly influence the estimated installation effects on load-bearing performance. This finding is consistent with previous studies [15, 26], which reported notable differences in numerically predicted load capacities when installation effects are omitted.

4. Conclusions and perspectives

This study presents a detailed analysis of the load–displacement behavior and failure mechanisms of tapered walls, validated through experimental centrifuge tests. LA and FEM using the MC model with associated flow rules provided comparable failure load predictions but underestimated experimental values. FEM analyses, utilizing both MC and HMC models, accurately captured load–displacement trends and stress distributions, while LA provided valuable insights into failure mechanisms and collapse loads.

Among all numerical approaches, the HMC model demonstrated the best performance in simulating bored pile behavior. This is likely due to its ability to represent nonlinear stress–strain behavior, stiffness degradation, and density-dependent strength in the sand, making it more suitable for simulating pile–soil interactions under varying stress paths.

The result shows the significant impact of taper geometry, with the moderately tapered wall achieving a better balance between shaft friction and base resistance. These differences are primarily attributed to installation-induced effects, such as soil densification, lateral stress increase, and stress redistribution, which were not taken into consideration in numerical analyses. These findings emphasize the importance of considering taper geometry and installation effects in the design and analysis of foundation systems, offering a validated framework for integrating numerical and experimental approaches in geotechnical engineering. The analyses were performed for walls under plane strain conditions. These conclusions can also be used to qualitatively describe the behavior of tapered piles.

The study reveals the importance of the dilatancy angle in the soil behavior and pile–soil interface. The use of associated flow with a high dilatancy angle reduces the gap between the behavior of the model and numerical simulation.

The perspective of this study is to improve the realism of numerical simulations, and future studies should incorporate pile installation effects using stepwise preloading or staged load application [18] to simulate stress build-up around the pile prior to loading. This simplified approach provides a practical alternative to more complex large deformation modeling techniques. Alternatively, more simplified techniques, such as applying initial stress fields with imposed lateral stress coefficient and prescribed stress distribution after installation, can also approximate the stress state without fully modeling the process. Here, one can use the contact stress distribution registered in centrifuge model tests. The perspective of this study could also be related to a more advanced analysis of the influence of interface parameters on the obtained numerical results. The interface shear tests with different boundary conditions, including constant volume tests, imposed constant normal stiffness of the interface, or other loading paths, can be performed to better simulate the soil–structure interaction and to determine the interface friction angle at a wide range of stress levels, plate roughness, and boundary conditions. Here, one can also consider ring shear tests to simulate large deformation during the continuous penetration of the wall.

Acknowledgments

The experimental results used in this manuscript were obtained within the TAPILES project (GEOLAB). This project has received funding from the European Union's Horizon 2020 research and innovation programme under Grant Agreement No. 101006512.

Funding information

Author states no funding involved.

Author contributions

The author confirms that all work – including conceptualization, methodology, investigation, writing (original draft and review), and visualization – was carried out solely by the author.

Conflict of interest statement

Author states no conflict of interest.

References

[1] Fahmy, A., El Naggar, M.H. (2017). Axial performance of helical tapered piles in sand. *Geotechnical and Geological Engineering*, *35*(4), 1549-1576. doi: 10.1007/s10706-017-0192-1.

[2] Naggar, M.H.E., Sakr, M. (2000). Evaluation of axial performance of tapered piles from centrifuge tests. *Canadian Geotechnical Journal*, *37*(6), 1295-1308. doi: 10.1139/t00-049.

[3] Sakr, M., Hesham El Naggar, M. (2003). Centrifuge modeling of tapered piles in sand. *Geotechnical Testing Journal*, *26*(1), 8935. doi: 10.1520/GTJ11106J.

[4] Wei, J., El Naggar, M.H. (1998). Experimental study of axial behaviour of tapered piles. *Canadian Geotechnical Journal*, *35*(4), 641-654. doi: 10.1139/t98-033.

[5] Randolph, M.F., Carter, J.P., Wroth, C.P. (1979). Driven piles in clay – The effects of installation and subsequent consolidation. *Géotechnique*, *29*(4), 361-393. doi: 10.1680/geot.1979.29.4.361.

[6] Robinsky, E.I., Morrison, C.F. (1964). Sand displacement and compaction around model friction piles. *Canadian Geotechnical Journal*, *1*(2), 81-93. doi: 10.1139/t64-002.

[7] Beijer Lundberg, A., Dijkstra, J., van Tol, F. (2012). *On the Modelling of Piles in Sand in the Small Geotechnical Centrifuge*. Delft University of Technology, Delft, The Netherlands, p. 10.

[8] Fu, S., Yang, Z.X., Jardine, R.J., Guo, N. (2023). Large-deformation finite-element simulation of deformation and strain fields resulting from closed-end displacement pile installation in sand. *Journal of Geotechnical and Geoenvironmental Engineering*, *149*(6), 04023038. doi: 10.1061/JGGEFK.GTENG-10480.

[9] Yi, J.T., Liu, F., Zhang, T.B., Yao, K., Zhen, G. (2021). A large deformation finite element investigation of pile group installations with consideration of intervening consolidation. *Applied Ocean Research*, *112*, 102698. doi: 10.1016/j.apor.2021.102698.

[10] Hamann, T., Qiu, G., Grabe, J. (2015). Application of a Coupled Eulerian–Lagrangian approach on pile installation problems under partially drained conditions. *Computers and Geotechnics*, *63*, 279-290. doi: 10.1016/j.compgeo.2014.10.006.

[11] Konkol, J., Bałachowski, L. (2017). Influence of installation effects on pile bearing capacity in cohesive soils – large deformation analysis via finite element method. *Studia Geotechnica et Mechanica*, *39*(1), 27-38. doi: 10.1515/sgem-2017-0003

[12] Yu, H., Zhou, H., Sheil, B., Liu, H. (2022). Finite element modelling of helical pile installation and its influence on uplift capacity in strain softening clay. *Canadian Geotechnical Journal*, *59*(12), 2050-2066. doi: 10.1139/cgj-2021-0527.

[13] Galavi, V., Martinelli, M. (2024). MPM simulation of the installation of an impact-driven pile in dry sand and subsequent axial bearing capacity. *Journal of Geotechnical and Geoenvironmental Engineering*, *150*(4), 04024019. doi: 10.1061/JGGEFK.GTENG-11592.

[14] Gao, L., Guo, N., Yang, Z. X., Jardine, R. J. (2022). MPM modeling of pile installation in sand: Contact improvement and quantitative analysis. *Computers and Geotechnics*, *151*, 104943. doi: 10.1016/j.compgeo.2022.104943.

[15] Phuong, N.T.V., Tol, A.F., van Elkadi, A.S.K., Rohe, A. (2016). Numerical investigation of pile installation effects in sand using material point method. *Computers and Geotechnics*, *73*, 58-71. doi: 10.1016/j.compgeo.2015.11.012.

[16] Duan, N., Cheng, Y.P., Lu, M., Wang, Z. (2021). DEM investigation of sand response during displacement pile installation. *Ocean Engineering*, *230*, 109040. doi: 10.1016/j.oceaneng.2021.109040.

[17] Guo, N., Liu, H.F., Li, B.J., Yang, Z.X. (2024). DEM study of the stress fields around the closed-ended displacement pile driven in sand. *Canadian Geotechnical Journal*, *61*(3), 549-561. doi: 10.1139/cgj-2023-0025.

[18] Engin, H. K., Brinkgreve, R.B.J., Van Tol, A.F. (2015). Simplified numerical modelling of pile penetration - the press-replace technique: Simplified numerical modelling of pile penetration – PR technique. *International Journal for Numerical and Analytical Methods in Geomechanics*, *39*(15), 1713-1734. doi: 10.1002/nag.2376.

[19] Goudarzy, M., Lavasan, A. A. (2024). Challenges in numerical modelling of screw piles installation and vertical loading based on centrifuge testing. *ISSMGE*. doi: 10.53243/ECPMG2024-146.

[20] OPTUM Engineering. (2020). *OPTUM G2 User Manual*. https://www.optumengineering.com/.

[21] LimitState Ltd. (2021). *LimitState GEO User Manual*. https://www.limitstate.com/geo.

[22] Gilber, M., Smith, C. C., Haslam, I. W., Pritchard, T. J. (2010). Application of discontinuity layout optimization to geotechnical limit analysis problems. *Proceedings of the 7th European Conference on Numerical Methods in Geotechnical Engineering*.

[23] Bałachowski, L., Kabeta, W.F., Thorel, L., Blanc, M., Dubreucq, T. (2024). Centrifuge modelling of tapered wall jacked into medium dense sand. *New Developments on Structural Design. XVIII European Conference on Soil Mechanics and Geotechnical Engineering*, Lisbon.

[24] Schanz, T., Vermeer, P.A., Bonnier, P.G. (2019). The hardening soil model: Formulation and verification. In R.B.J. Brinkgreve (Ed.), *Beyond 2000 in Computational Geotechnics* (1st ed., pp. 281-296). CRC Press (Taylor & Francis Group), London, UK. doi: 10.1201/9781315138206-27.

[25] Andria-Ntoanina, I., Canou, J., Dupla, J. (2010). Caractérisation mécanique du sable de Fontainebleau NE34 à l'appareil triaxial sous cisaillement monotone. *Laboratoire Navier–Géotechnique. CERMES, ENPC/ LCPC*. Routledge, London, UK.

[26] Broere, W., Van Tol, A.F. (2006). Modelling the bearing capacity of displacement piles in sand. *Proceedings of the Institution of Civil Engineers – Geotechnical Engineering*, *159*(3), 195-206. doi: 10. 1680/geng.2006.159.3.195.